Article

Molecular Cell

Cryo-EM of Mitotic Checkpoint Complex-Bound APC/C Reveals Reciprocal and Conformational Regulation of Ubiquitin Ligation

Graphical Abstract

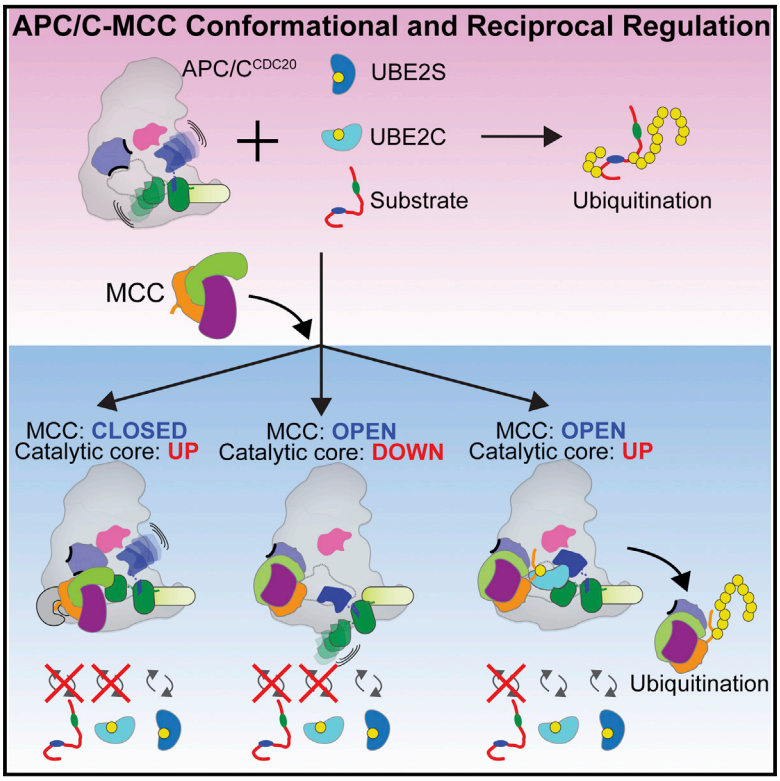

Highlights

- Cryo-EM shows reciprocal and conformational regulation of APC/C^{CDC20} and MCC
- MCC blocks APC/C^{CDC20}-binding sites for substrates such as Cyclins and Securin
- Closed APC/C^{CDC20}-MCC blocks E2 UBE2C, as during the spindle checkpoint
- Open APC/C^{CDC20}-MCC directs ubiquitination of MCC, as during checkpoint silencing

Authors

Masaya Yamaguchi, Ryan VanderLinden, Florian Weissmann, ..., Jan-Michael Peters, Holger Stark, Brenda A. Schulman

Correspondence

jan-michael.peters@imp.ac.at (J.-M.P.), hstark1@gwdg.de (H.S.), brenda.schulman@stjude.org (B.A.S.)

In Brief

The mitotic checkpoint complex (MCC) prevents APC/C^{CDC20}-catalyzed ubiquitination of anaphase inhibitors until all chromosomes are properly bioriented. Cryo-EM and biochemistry reveal that diverse conformations of APC/C^{CDC20}-MCC regulate E2 activation and ubiquitin targeting to ensure accurate chromosome segregation.

Accession Numbers

5KHR
5KHU

Yamaguchi et al., 2016, Molecular Cell *63*, 593–607
August 18, 2016
http://dx.doi.org/10.1016/j.molcel.2016.07.003

Molecular Cell
Article

Cryo-EM of Mitotic Checkpoint Complex-Bound APC/C Reveals Reciprocal and Conformational Regulation of Ubiquitin Ligation

Masaya Yamaguchi,[1,6] Ryan VanderLinden,[1,2,6] Florian Weissmann,[3,6] Renping Qiao,[3] Prakash Dube,[4] Nicholas G. Brown,[1] David Haselbach,[4] Wei Zhang,[5] Sachdev S. Sidhu,[5] Jan-Michael Peters,[3,*] Holger Stark,[4,*] and Brenda A. Schulman[1,2,*]

[1]Department of Structural Biology, St. Jude Children's Research Hospital, Memphis, TN 38105, USA
[2]Howard Hughes Medical Institute, St. Jude Children's Research Hospital, Memphis, TN 38105, USA
[3]Research Institute of Molecular Pathology (IMP), Vienna Biocenter (VBC), 1030 Vienna, Austria
[4]Max Planck Institute for Biophysical Chemistry, 37077 Göttingen, Germany
[5]Donnelly Centre for Cellular and Biomolecular Research and Banting and Best Department of Medical Research, University of Toronto, Toronto, ON M5S3E1, Canada
[6]Co-first author
*Correspondence: jan-michael.peters@imp.ac.at (J.-M.P.), hstark1@gwdg.de (H.S.), brenda.schulman@stjude.org (B.A.S.)
http://dx.doi.org/10.1016/j.molcel.2016.07.003

SUMMARY

The mitotic checkpoint complex (MCC) coordinates proper chromosome biorientation on the spindle with ubiquitination activities of CDC20-activated anaphase-promoting complex/cyclosome (APC/C^{CDC20}). APC/C^{CDC20} and two E2s, UBE2C and UBE2S, catalyze ubiquitination through distinct architectures for linking ubiquitin (UB) to substrates and elongating polyUB chains, respectively. MCC, which contains a second molecule of CDC20, blocks APC/C^{CDC20}-UBE2C-dependent ubiquitination of Securin and Cyclins, while differentially determining or inhibiting CDC20 ubiquitination to regulate spindle surveillance, checkpoint activation, and checkpoint termination. Here electron microscopy reveals conformational variation of APC/C^{CDC20}-MCC underlying this multifaceted regulation. MCC binds APC/C-bound CDC20 to inhibit substrate access. However, rotation about the CDC20-MCC assembly and conformational variability of APC/C modulate UBE2C-catalyzed ubiquitination of MCC's CDC20 molecule. Access of UBE2C is limiting for subsequent polyubiquitination by UBE2S. We propose that conformational dynamics of APC/C^{CDC20}-MCC modulate E2 activation and determine distinctive ubiquitination activities as part of a response mechanism ensuring accurate sister chromatid segregation.

INTRODUCTION

The massive, multisubunit E3 ligase anaphase-promoting complex/cyclosome (APC/C) initiates chromosome segregation by directing ubiquitin (UB)-mediated proteolysis of anaphase inhibitors, such as Securin, and other key mitotic regulators like Cyclins. Regulation is achieved by post-translational modifications and the coordinated action of coactivators, E2 enzymes, and inhibitors (Sivakumar and Gorbsky, 2015). APC/C is activated in prophase by phosphorylation, which allows binding to the coactivator CDC20 (Fujimitsu et al., 2016; Qiao et al., 2016; Zhang et al., 2016). CDC20 binding enables substrate binding, and it allosterically activates the catalytic core consisting of cullin (APC2) and RING (APC11) subunits (Burton et al., 2005; Chang et al., 2014; Kimata et al., 2008; Van Voorhis and Morgan, 2014; Zhang et al., 2016).

APC2 and APC11 are differentially harnessed by evolving ubiquitinated substrates and APC/C's two partner E2s, UBE2C and UBE2S, for different forms of polyubiquitination (Brown et al., 2016), with UBE2C catalyzing UB ligation directly to substrates and UBE2S extending K11-linked chains. However, accurate cell division depends on APC/C^{CDC20} waiting until all chromosomes are properly bioriented on the spindle before triggering destruction of anaphase inhibitors (Jia et al., 2013; Primorac and Musacchio, 2013). Premature chromosome segregation and aneuploidy are averted by the spindle assembly checkpoint (SAC). The SAC monitors chromosome attachment and delays anaphase by producing the mitotic checkpoint complex (MCC), which blocks APC/C^{CDC20}-dependent ubiquitination of substrates such as Securin and Cyclin B (Braunstein et al., 2007; Burton and Solomon, 2007; Fraschini et al., 2001; Hardwick et al., 2000; Herzog et al., 2009; Izawa and Pines, 2015; Kulukian et al., 2009; Sudakin et al., 2001).

Control of APC/C^{CDC20} activity in response to the status of the mitotic spindle involves tunable cycles of CDC20 synthesis and degradation, MCC assembly and disassembly, and APC/C^{CDC20}-MCC association and dissociation (Foley and Kapoor, 2013; Foster and Morgan, 2012; Jia et al., 2013; Kim and Yu, 2011; Lara-Gonzalez et al., 2012; London and Biggins, 2014; Mansfeld et al., 2011; Musacchio, 2015; Musacchio and Ciliberto, 2012; Primorac and Musacchio, 2013; Uzunova et al., 2012). During chromosome alignment, APC/C^{CDC20} remains blocked by newly produced MCC replacing that which has

dissociated. Checkpoint activation results in stabilization of MCC and APC/C^{CDC20}-MCC complexes, whereas proper chromosome biorientation leads to termination of MCC production, liberation of APC/C^{CDC20}, and dismantling of MCC.

A particularly vexing feature of checkpoint regulation is the reciprocal control of APC/C^{CDC20} and MCC (Reddy et al., 2007; Varetti et al., 2011). The evolutionarily conserved MCC core is a three-protein complex consisting of a distinct molecule of CDC20, MAD2, and BUBR1/Mad3, although MCC from some organisms, including humans, also contains BUB3 (Izawa and Pines, 2015; Jia et al., 2013; Primorac and Musacchio, 2013). On one hand, MCC acts as an inhibitor of APC/C^{CDC20} and blocks substrates. However, MCC appears to modulate activity of the priming E2, UBE2C, without impacting binding to the chain-forming E2, UBE2S (Kelly et al., 2014).

In the context of an APC/C^{CDC20}-MCC complex, CDC20 can be ubiquitinated depending on the status of the checkpoint (Eytan et al., 2013; Ge et al., 2009; Jia et al., 2011, 2013; Mansfeld et al., 2011; Miniowitz-Shemtov et al., 2010; Musacchio, 2015; Musacchio and Ciliberto, 2012; Nilsson et al., 2008; Pan and Chen, 2004; Reddy et al., 2007; Uzunova et al., 2012; Varetti et al., 2011). Although CDC20 is a very short-lived protein, mechanisms and consequences of CDC20 ubiquitination remain under investigation. Ubiquitination may prevent accumulation of excess CDC20, potentially to avert mitotic slippage (Mansfeld et al., 2011; Nilsson et al., 2008). However, high UBE2C activity correlates with CDC20 ubiquitination and MCC dissociation from APC/C, suggesting that UBE2C-mediated CDC20 ubiquitination contributes to checkpoint termination (Foster and Morgan, 2012; Reddy et al., 2007; Uzunova et al., 2012; Varetti et al., 2011). Accordingly, knocking down UBE2C and UBE2S decreased the efficiency of release from the SAC and delayed progress from nuclear envelope breakdown to anaphase (Garnett et al., 2009; Jia et al., 2011; Kelly et al., 2014; Varetti et al., 2011; Wild et al., 2016; Williamson et al., 2009). Furthermore, CDC20 was stabilized and MCC accumulated on APC/C in checkpoint-arrested cells depleted for the APC15 subunit, or the corresponding Mnd2 in yeast (Foster and Morgan, 2012; Mansfeld et al., 2011; Uzunova et al., 2012). Notably, the only obvious catalytic defect of APC/C lacking APC15 (APC/CΔ15) was strikingly impaired CDC20 ubiquitination in the presence of MCC (Foster and Morgan, 2012; Uzunova et al., 2012).

Here we use electron microscopy (EM) and biochemistry to dissect regulation of APC/C^{CDC20} and MCC via ubiquitination by UBE2C and UBE2S. For clarity, we refer to the APC/C-bound activator CDC20 as $CDC20_A$ (i.e., in APC/C^{CDC20}) and that in MCC as $CDC20_M$. While MCC uniformly blocks substrate binding to APC/C^{CDC20}, multiple conformations of APC/C^{CDC20}-MCC, with rotation of the $CDC20_A$-MCC assembly relative to APC/C and different positions for the APC2-APC11 catalytic core, determine if $CDC20_M$ is a substrate of UBE2C. Notably, the distribution of MCC complexes with APC/C^{CDC20} lacking APC15 (APC/C^{CDC20}Δ15) is shifted toward configurations that block UBE2C activation, while UBE2S binding and di-UB synthesis capabilities remain intact to presumably mediate rapid polyubiquitination after CDC20 is modified by UBE2C. We propose that biasing APC/C^{CDC20}-MCC conformation toggles ubiquitination of CDC20 as part of a dynamic response mechanism that can either sustain the SAC or trigger rapid onset of anaphase.

RESULTS

EM Reconstructions Reveal Conformational Variability of APC/C^{CDC20}-MCC

We established recombinant systems for APC/C^{CDC20} (with glutamate replacements for 100 Ser/Thr sites of mitotic phosphorylation) that mimics the endogenous complex (Qiao et al., 2016; Weissmann et al., 2016), and for MCC by coexpressing its subunits in insect cells (Figures S1A–S1C). This allowed reconstituting MCC inhibition of UB ligation to fluorescent versions of Cyclin B's N-terminal domain ($CycB^{N*}$), Securin*, and Cyclin A* by APC/C^{CDC20}, UBE2C, and UBE2S (Figure 1A).

To gain structural insights into regulation, we analyzed APC/C^{CDC20}-MCC by cryo-EM. Three-dimensional (3D) classification revealed several sub-populations with two globally distinctive configurations we termed "closed" and "open", which themselves are defined by multiple classes presumably reflecting their conformational dynamics. Cryo-EM reconstructions for APC/C^{CDC20}-MCC in the closed and open configurations were refined at resolutions of 9 and 10 Å, respectively (Table S1). Docking prior structures of human APC/C^{CDC20} and *S. pombe* MCC core (44% identical to human CDC20-BUBR1-MAD2) into the maps showed the arrangements of the two molecules of CDC20, with A bound to APC/C via activator-binding sites and the other (M) in MCC (Chao et al., 2012; Izawa and Pines, 2015; Primorac and Musacchio, 2013; Zhang et al., 2016).

The distinct conformations display substantially different orientations of $CDC20_A$-MCC with respect to APC/C (Figures 1B and 1C; Movies S1 and S2). In the closed conformation, MCC fills the central cavity by engaging APC/C^{CDC20} on three sides. A continuous surface from $CDC20_M$ and BUBR1 engages CDC20A. $CDC20_M$ contacts the available protomer (A) of the APC8 homodimer. BUBR1 interacts with the APC2-APC11 cullin-RING catalytic core. When open, the $CDC20_A$-MCC assembly is preserved but is localized away from the catalytic core.

Only the MCC core corresponding to CDC20-BUBR1-MAD2 was readily visible in the maps, despite the presence of BUB3 in the complex (Figure S1A). To validate this, we purified an MCC core complex that inhibited substrate ubiquitination as described (Izawa and Pines, 2015), with only slightly lower efficiency than full MCC in our assays (Figure 1A). Upon performing side-by-side negative-stain EM analyses on APC/C^{CDC20} bound to full or core MCC, the resultant maps were superimposable, and there were not obvious major differences in the ratios of closed and open configurations among matched preps with or without BUB3 (Figures 1D–1G and S1B–S1D). For comparison, retrospective inspection of the EM map from endogenous APC/C^{CDC20}-MCC further validated that only the MCC core is apparent, even in the presence of BUB3 (Figure 1H) (Herzog et al., 2009). This is consistent with conservation of key APC/C^{CDC20}-MCC features across eukaryotes, as MCC lacks BUB3 in some organisms (Vanoosthuyse et al., 2009; Windecker et al., 2009). We speculate that BUB3 may be relatively flexibly tethered to APC/C^{CDC20}-MCC, and, thus, all subsequent EM studies were performed with the MCC core complex unless otherwise stated (Table S1).

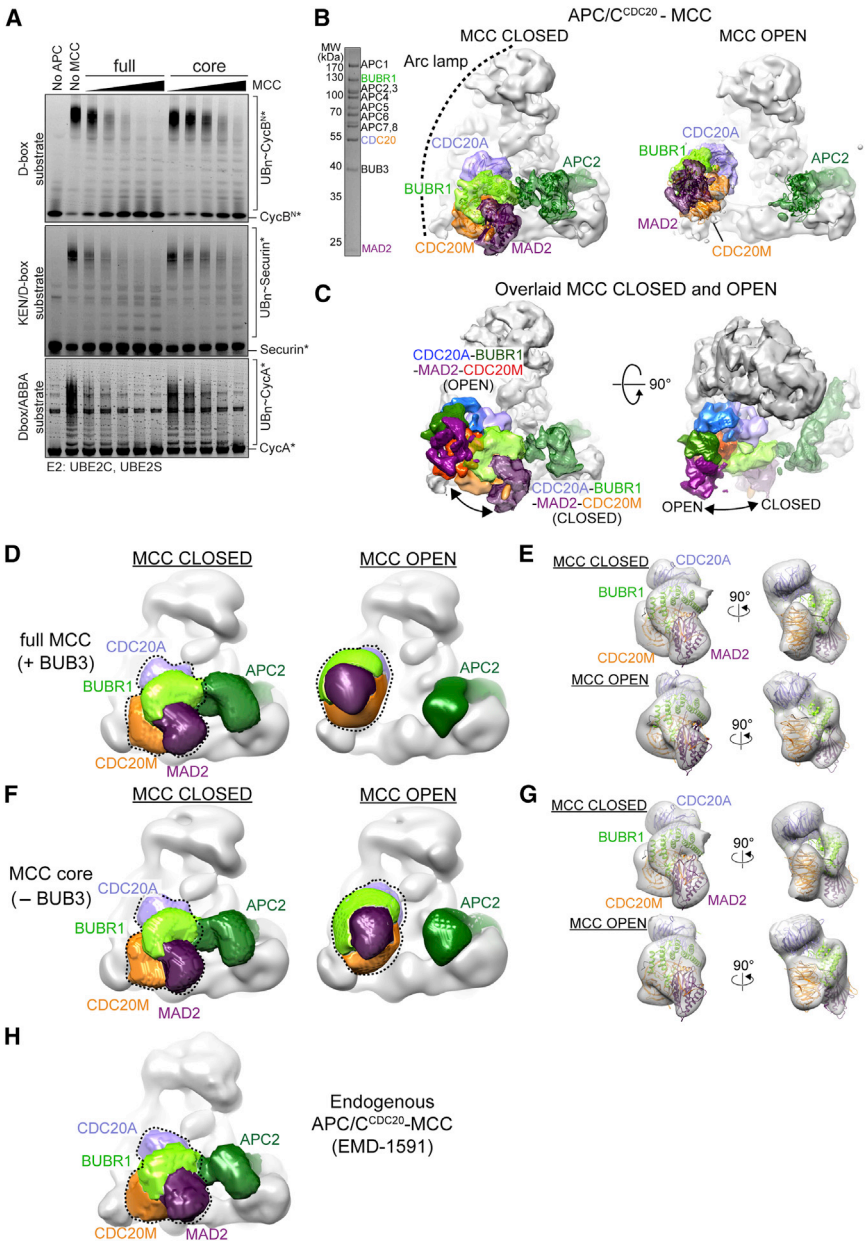

Figure 1. Multiple APC/C^{CDC20}-MCC Conformations Revealed by EM

(A) Ubiquitination of fluorescent CycB^{N}*, Securin*, and CycA* by APC/C^{CDC20}, titrating increasing concentrations of either full or core (CDC20$_M$-BUBR1-MAD2) MCC, is shown.

(B) Cryo-EM reconstructions show representative APC/C^{CDC20}-MCC closed (left) and open (right) conformations refined at 9- and 10-Å resolution, respectively (SDS-PAGE gel of APC/C^{CDC20}-MCC, left).

(C) Superimposition of cryo-EM maps for closed and open conformations of APC/C^{CDC20}-MCC is shown.

(D) Negative-stain EM reconstructions show APC/C^{CDC20} in complex with full MCC, which contains BUB3.

(E) The overall CDC20$_A$-MCC core assembly from docked crystal structures (Chao et al., 2012; Tian et al., 2012) is observed in both the closed and open configurations of APC/C^{CDC20}-MCC.

(F) Shown as in (D), except with core MCC (CDC20$_M$-BUBR1-MAD2) lacking BUB3.

(G) Shown as in (E), except with CDC20$_A$-MCC core assembly-docked negative-stain EM maps from (F).

(H) Negative-stain EM reconstruction of endogenous MCC-bound APC/C (Electron Microscopy Data Bank: EMD-1591) (Herzog et al., 2009) is shown.

See also Figure S1, Tables S1 and S2, and Movies S1, S2, and S3.

Reexamination of the published negative-stain EM map of APC/C-MCC purified from checkpoint-arrested HeLa cells revealed that the dominant population (56%) corresponds to the closed configuration, which may reflect higher propensity for purification due to additional contacts, increased homogeneity of the closed configuration, or relative stabilization of the closed configuration during the checkpoint (Figure 1H) (Herzog et al., 2009). Blurring of the MCC moiety in the published map generated from unstained cryo-EM data on endogenous APC/C^{CDC20}-MCC may reflect conformational heterogeneity arising from the dynamic configurations (Herzog et al., 2009). Superimposing the EM maps corresponding to different 3D classes suggested a continuum of conformations where the CDC20$_A$-MCC assembly rotates to APC/C. Notably, the APC2-APC11 catalytic core also exhibited conformational heterogeneity between the closed and open configurations and among open 3D classes even from a single sample (Movie S3).

MCC Inhibition of Substrate Ubiquitination Revealed by Side-by-Side Comparison of APC/C and APC/C^{CDC20} Complexes with Substrate or MCC

Cryo-EM reconstructions were aligned for phosphorylated apo APC/C (Figure 2A) (Zhang et al., 2016), substrate-bound APC/C^{CDC20} (Figure 2B) (Zhang et al., 2016), and closed and open conformations of APC/C^{CDC20}-MCC (Figures 2C and 2D). Side-by-side comparison showed common mechanisms by which the closed and open configurations hijack substrate-binding sites on APC/C^{CDC20}, while differing in their interactions with the catalytic core.

Prior structural data showed how CDC20 can allosterically activate E3 ligase activity. In the absence of CDC20, the canonical E2-binding site on APC11's RING domain is masked, because the APC2-APC11 cullin-RING catalytic core occupies a down position (Figure 2A) (Chang et al., 2014). However, in the cryo-EM maps for an APC/C^{CDC20}-substrate complex, the APC2-APC11 catalytic core is relatively up and freed from autoinhibition, and it is visible only at lower contour and

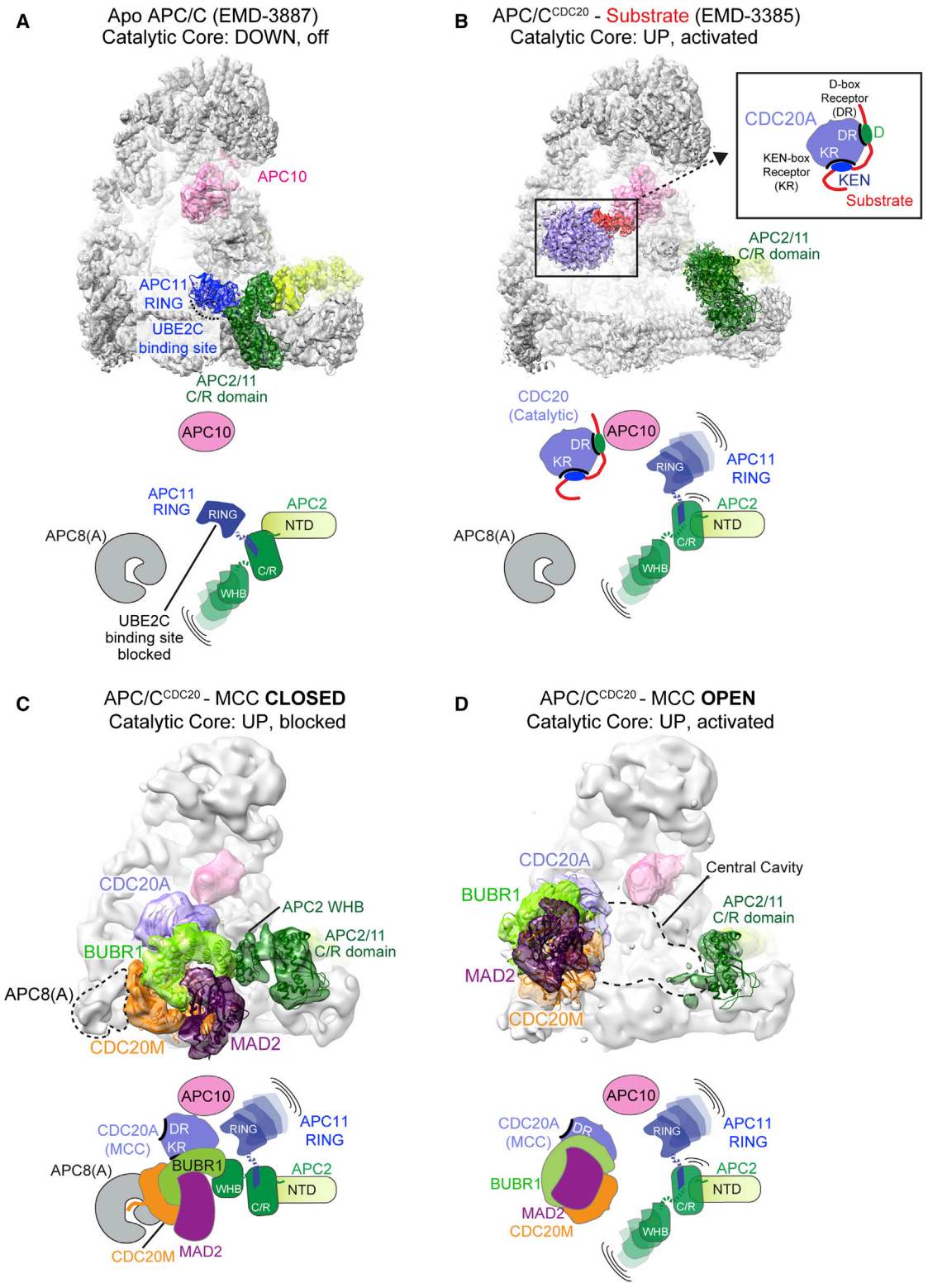

Figure 2. Snapshots of Distinct APC/C Conformations Associated with Activation by CDC20 and Modulation by MCC

(A) Prior cryo-EM map of apo-phosphorylated APC/C (Zhang et al., 2016) showed the APC2 (green)-APC11 (blue) catalytic core as down, blocking the canonical E2-binding site on APC11's RING used by UBE2C. Cartoon depicts key elements related to MCC functions.

(legend continued on next page)

resolution presumably due to mobility (Figure 2B) (Zhang et al., 2016). This increases catalytic competence, because three domains of the catalytic core (the intermolecular cullin/RING C/R domain, the APC2 C-terminal WHB domain, and the APC11 C-terminal RING domain) are harnessed into different catalytic architectures for substrate ubiquitination by UBE2C and UB chain elongation by UBE2S (Brown et al., 2015, 2016; Chang et al., 2015).

In the closed configuration, MCC captures the WHB domain from APC2, which is enabled by upward positioning of the C/R domain (Figure 2C). When APC/C^{CDC20}-MCC is open, the catalytic core is fully available, localized upward, and less visible, consistent with competence for binding to UBE2C (Figure 2D) (Brown et al., 2015, 2016; Chang et al., 2015).

In both configurations, MCC masks substrate-binding sites by $CDC20_M$ and BUBR1 encasing the top side of $CDC20_A$'s β-propeller (Figures 1 and 2). Also, relative rotation of $CDC20_A$'s β-propeller dismantles the D-box-binding site between $CDC20_A$ and APC10 (Figures 2B–2D) (Herzog et al., 2009).

In separate sections below, we describe EM data (Table S1) and biochemistry defining elements mediating MCC inhibition of APC/C^{CDC20}, mechanisms of CDC20 ubiquitination in the context of APC/C^{CDC20}-MCC, and how APC/C^{CDC20}-MCC structure and activity are modulated in the absence of APC15.

APC/C^{CDC20}-MCC Elements Inhibiting Substrate Ubiquitination

The highest resolution cryo-EM map obtained during the course of these studies was for the closed configuration with an APC/C^{CDC20} mutant lacking APC15 (Figure S2A; Table S1; 4.8-Å resolution by gold-standard Fourier shell correlation). Here we depict the $CDC20_A$-MCC interface from this map, while effects of deleting APC15 are described in separate sections. Lower resolution for the $CDC20_A$-MCC assembly of ≈6.5 Å presumably reflects relative mobility, but it was sufficient to dock prior high-resolution structures of MCC subunits for visualizing elements mimicking substrate D-, KEN-, and ABBA/Phe-box motifs (Figures 3, S2, and S3).

On one edge of $CDC20_A$, there is potentially weak density in the D-box-binding site, and strong density for a Cys-Arg-Tyr (CRY) box immediately preceding $CDC20_M$'s propeller domain (Figures 3A and 3B). The other edge of $CDC20_A$ apparently binds an ABBA/Phe-box-like motif (Di Fiore et al., 2015; Diaz-Martinez et al., 2015), which continues into a pre-KEN sequence and ultimately a KEN-box that are sandwiched between the $CDC20_A$ propeller and the $CDC20_M$/BUBR1 surface from MCC (Figures 3A, 3C, and S3A). Indeed, prior studies had identified D1 and KEN2 motifs in BUBR1 and the corresponding D- and KEN-box receptor sites on $CDC20_A$ as important for MCC binding to APC/C (Izawa and Pines, 2015). We further validated the cryo-EM data by testing effects of mutating BUBR1's D1, ABBA-like, pre-KEN, and KEN2 motifs and $CDC20_M$'s CRY box in MCC, as well as the KEN receptor in $CDC20_A$. All these structure-based mutations thwarted MCC inhibition of substrate ubiquitination (Figures 3D, 3E, and S3B).

APC/C^{CDC20}-MCC in the Open Configuration Is Structurally Poised for UBE2C-Dependent Ubiquitination of $CDC20_M$

The two APC/C^{CDC20}-MCC conformations present an intriguing dichotomy for the catalytic core. In particular, with the $CDC20_A$-MCC assembly swung open, APC/C's central cavity is vacant and, in principle, could accommodate UBE2C (Figure 2D) (Brown et al., 2015; Chang et al., 2015). Although previous studies monitoring cellular CDC20 ubiquitination during the spindle assembly checkpoint could not distinguish between $CDC20_A$ and $CDC20_M$ (Foster and Morgan, 2012; Mansfeld et al., 2011; Uzunova et al., 2012), we used methylated UB that cannot form chains to directly probe targeting. $CDC20_A$ was distinguished by an N-terminal Myc tag and $CDC20_M$ by a FLAG tag (Figure 4A). Adding MCC to APC/C^{CDC20} and the E2 UBE2C resulted in $CDC20_M$ ubiquitination and decreased modification of $CDC20_A$ (Figure 4B). $CDC20_M$ ubiquitination was decreased by mutating a pair of known CDC20 ubiquitination sites (Lys485 and 490) within MCC (Figure 4C) (Mansfeld et al., 2011; www.phosphosite.org).

To visualize the APC/C^{CDC20}-MCC-UBE2C architecture poised for $CDC20_M$ ubiquitination, we modified our published approach to capture targeting by UBE2C (Brown et al., 2015, 2016). Briefly, the homobifunctional crosslinker BMOE joined UBE2C's active site Cys with a Cys corresponding to Lys490 in a modified $CDC20_M$ (Figure 4D). A purified BMOE-linked MCC-UBE2C complex was assembled with APC/C^{CDC20} for structural analysis by negative-stain EM (Figures 4D and 4E). The EM reconstruction shows the open configuration. Docking prior crystal structures shows how APC2's WHB and APC11's RING domains co-engage UBE2C (Brown et al., 2014, 2015). This places UBE2C in a parallel location as poised for substrate ubiquitination, except UBE2C's active site is juxtaposed with $CDC20_M$ (Figures 4E and S4) (Brown et al., 2015; Chang et al., 2015). We mutationally tested the mechanism, removing APC2's UBE2C-binding WHB domain or APC11's UBE2C-activating RING domain from APC/C^{CDC20}, or with UBE2C F53D and Y91D point mutations in the APC2- and APC11-binding sites, respectively (Brown et al., 2014, 2015). The mutants eliminated $CDC20_M$ ubiquitination, suggesting a crucial role for the APC2-APC11 cullin-RING mechanism activating UBE2C∼UB (Figures 4F and S4) (Brown et al., 2015).

(B) Prior cryo-EM map for APC/C^{CDC20}-substrate complex (Zhang et al., 2016), showing substrate D-box (red) co-recruited to CDC20's propeller (violet) and APC10 (pink). The catalytic core is activated by increased conformational mobility. D-box receptor (DR) and KEN-box receptor (KR) sites are indicated.

(C) Cryo-EM map showing closed configuration of APC/C^{CDC20}-MCC. MCC blocks substrate-binding sites and contacts APC2's UBE2C-binding WHB domain and APC8 (protomer A).

(D) Cryo-EM map showing open configuration of APC/C^{CDC20}-MCC. MCC blocks substrate-binding sites. APC/C's central cavity is vacant and APC2-APC11 catalytic core is activated and less resolved, suggestive of mobiltity.

See also Figure S2.

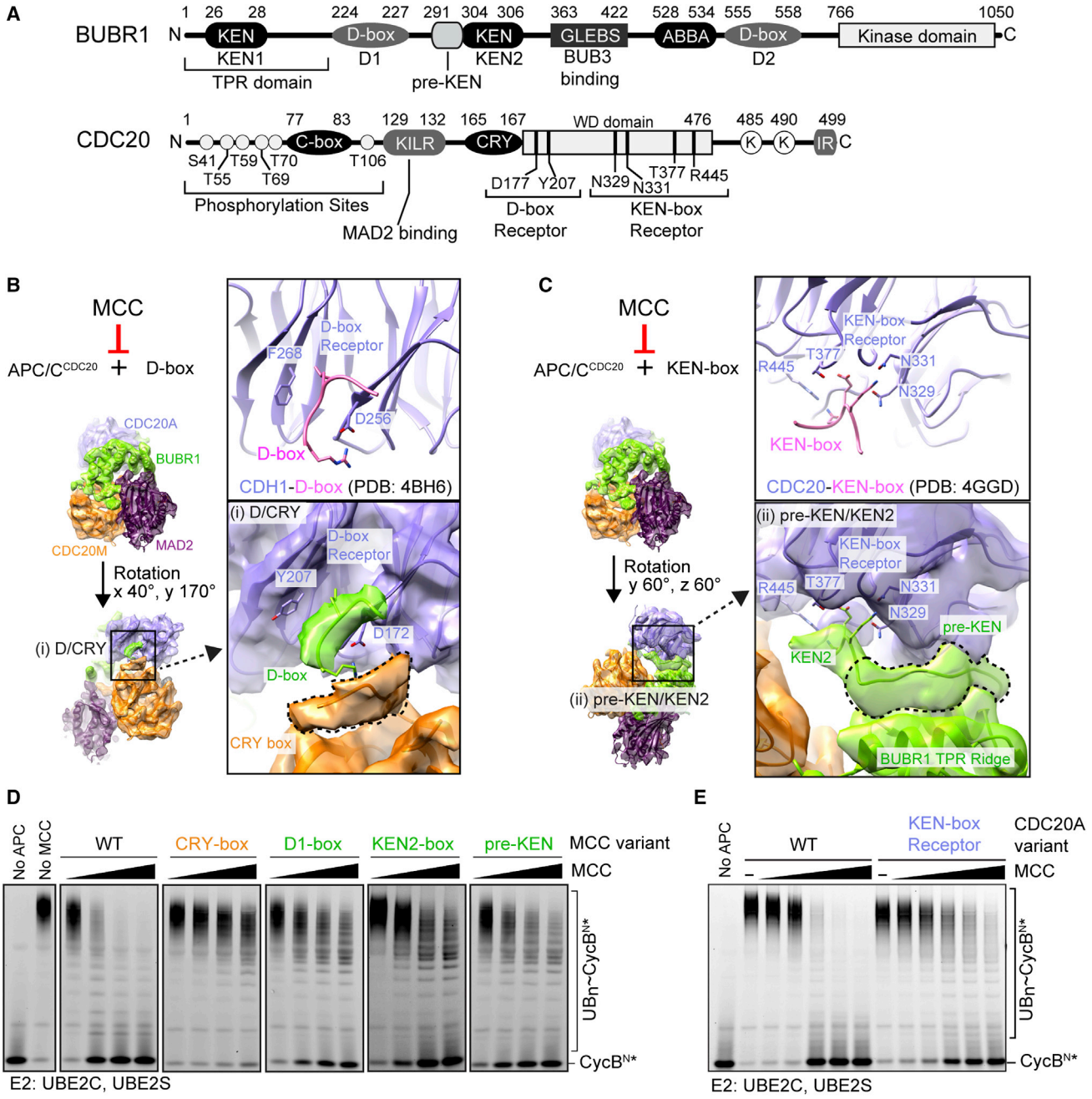

Figure 3. Multiple Related Elements Mediate Substrate and MCC Association with $CDC20_A$

(A) Schemes of BUBR1 and CDC20 motifs are shown.

(B) Close-up views of coactivator-D/CRY-box interactions are aligned for crystal structure of CDH1-D-box (He et al., 2013) and cryo-EM map of APC/C^{CDC20}Δ15-MCC (closed, 4.8-Å resolution) to show density for $CDC20_M$ CRY-box and D-box receptor region of $CDC20_A$.

(C) Close-up views show CDC20-KEN-box interactions aligned from crystal structure (Tian et al., 2012) and cryo-EM map of APC/C^{CDC20}Δ15-MCC (closed configuration, 4.8-Å resolution).

(D) Mutations in key MCC elements impair inhibition, detected by titrating increasing concentrations of MCC into reactions monitoring APC/C^{CDC20}-mediated ubiquitination of the fluorescent substrate $CycB^{N*}$.

(E) Mutations in $CDC20_A$ KEN-box-binding site impair MCC-mediated inhibition, detected by reactions as in (D). Note that $CycB^{N*}$ has a D-box, but not a KEN-box, so its ubiquitination in the absence of MCC is not substantially impaired by $CDC20_A$ KEN-box receptor mutant.

See also Figure S3.

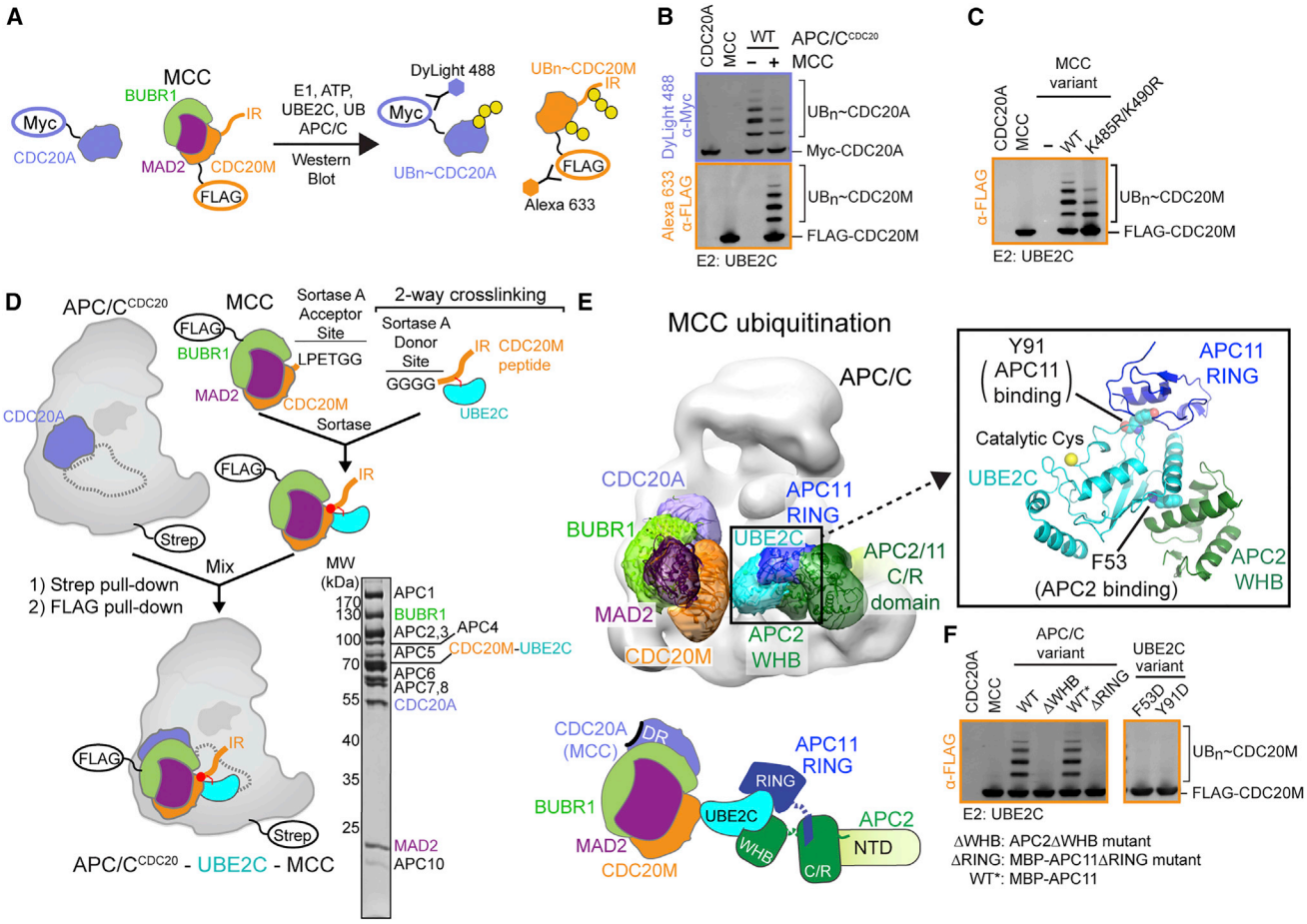

Figure 4. APC/C^{CDC20}-MCC Open Configuration Directs UBE2C-Catalyzed Ubiquitination of CDC20$_M$

(A) Scheme shows two-color western blot distinguishing CDC20$_A$ and CDC20$_M$ in ubiquitination assays.

(B) APC/C^{CDC20} and UBE2C-dependent modification of CDC20 was monitored in reactions with methyl-UB that can be linked to substrate, but cannot form chains.

(C) Reactions as in (B) show roles of known CDC20 ubiquitination sites by comparing APC/C^{CDC20} and UBE2C-dependent ubiquitination for WT and K485R/K490R CDC20$_M$.

(D) Scheme for purifying APC/C^{CDC20}-UBE2C-MCC core, with CDC20$_M$ residue 490 (corresponding to ubiquitination site) crosslinked to active site of UBE2C, is shown.

(E) Negative-stain EM reconstruction of APC/C^{CDC20}-UBE2C-MCC core representing CDC20$_M$ ubiquitination, with CDC20$_A$-MCC rotated in the open configuration. Inset: close-up of model shows key elements to recruit/activate/position UBE2C from prior crystal structures that are docked in EM map (Brown et al., 2014, 2015).

(F) Assay as in (B) tested cullin (APC2) and RING (APC11) architecture in recruiting/positioning/activating UBE2C for UB ligation to CDC20$_M$, through deleting UBE2C-binding (APC2 WHB) and -activating (APC11 RING) domains from APC/C, or mutating corresponding contact residues from UBE2C (F53 and Y91, respectively) (Brown et al., 2014).

See also Figure S4.

Cryo-EM Maps of APC/C^{CDC20}-MCC without the APC15 Subunit Show a Shift toward Conformations Inhibiting the Activation of UBE2C

To understand how APC/C^{CDC20}-MCC can be regulated, we considered that depleting the APC/C subunit APC15 selectively impairs CDC20 ubiquitination during checkpoint regulation (Foster and Morgan, 2012; Mansfeld et al., 2011; Uzunova et al., 2012). We discovered this is an intrinsic property of APC/C, because, in comparison to the wild-type (WT) complex, recombinant APC/C^{CDC20} prepared without APC15 (APC/C^{CDC20}Δ15) retained substrate ubiquitination activity that was inhibited by MCC, but MCC ubiquitination was selectively impaired (Figures 5A, 5B, and S5A).

To compare structural effects of deleting APC15 on substrate ubiquitination versus on interactions with MCC, we first adapted our method for visualizing an assembly mimicking an APC/C^{CDH1}-UBE2C∼UB-substrate intermediate (Brown et al., 2015). We determined a cryo-EM reconstruction of APC/C^{CDC20}Δ15 bound to a three-way crosslinked complex linking the preferred ubiquitination site in a substrate, UBE2C, and a donor UB (6.1-Å resolution, gold-standard Fourier shell correlation; Figures 5C and S5B). In the maps, the most static regions extend to ≈4 Å

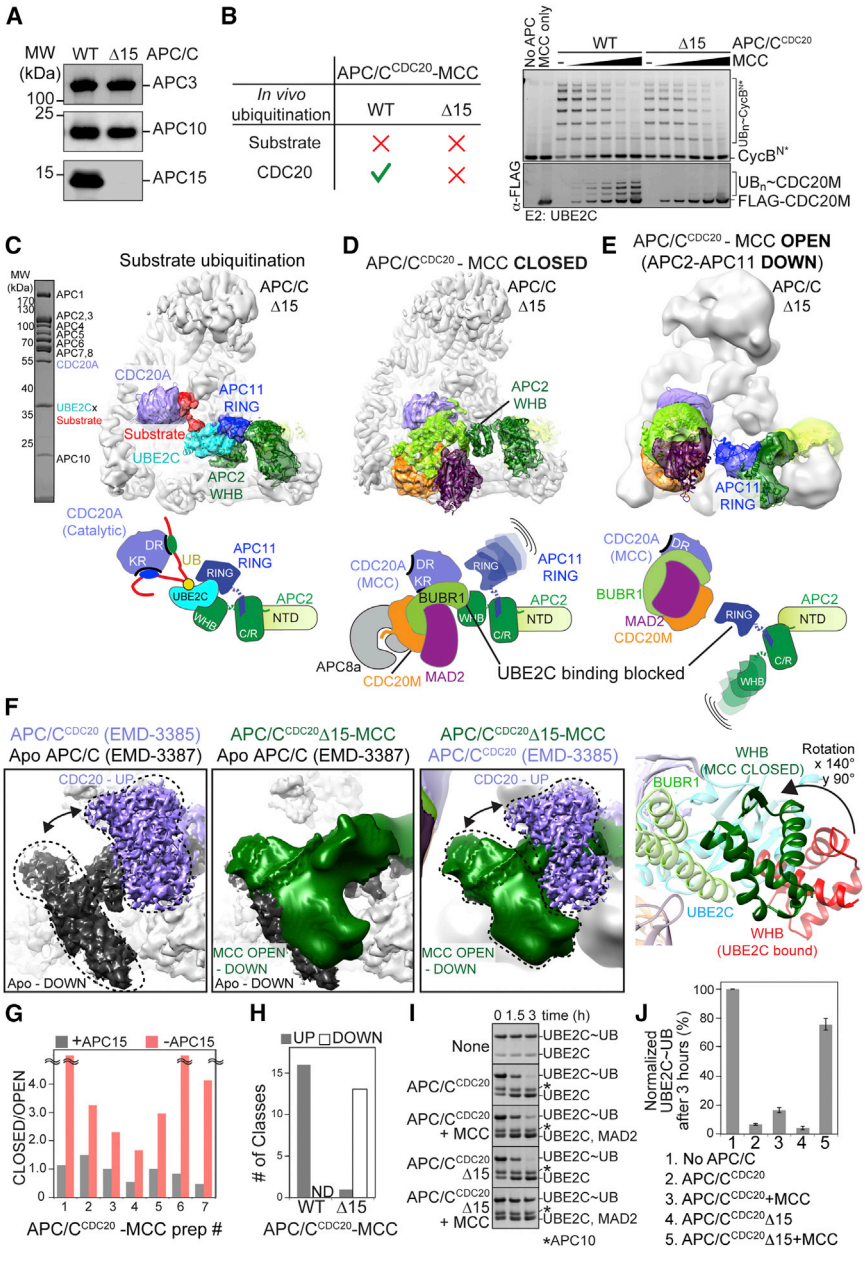

Figure 5. Deletion of APC15 Influences APC/C^{CDC20}-MCC Conformational Regulation and Activity with the E2 UBE2C

(A) Western blots (anti-APC3, -APC10, and -APC15) confirm lack of APC15 in recombinant APC/C^{CDC20}Δ15 compared to WT control.

(B) Recombinant APC/C^{CDC20}Δ15 recapitulates key endogenous properties. Left: summary from Foster and Morgan (2012), Mansfeld et al. (2011), and Uzunova et al. (2012) is shown. Right: deleting APC15 from recombinant APC/C^{CDC20} has no obvious impact on UBE2C-dependent substrate ubiquitination in the absence of MCC but impairs ubiquitination of CDC20$_M$ from MCC, tested by simultaneous detection of fluorescent CycB^{N*} substrate and FLAG-CDC20$_M$ in reaction.

(C) Cryo-EM map of APC/C^{CDC20}Δ15 complex representing substrate ubiquitination with UBE2C (UBE2C active site crosslinked to substrate, 6.1-Å resolution, SDS-PAGE gel, left). Cartoon of catalytic architecture for substrate ubiquitination is shown below.

(D) Cryo-EM map shows APC/C^{CDC20}Δ15-MCC in closed configuration (4.8-Å resolution), resolving elements blocking substrate binding and inhibiting APC/C catalytic core in the up (activated) position.

(E) Cryo-EM map showing APC/C^{CDC20}Δ15-MCC in distinctive open configuration (9-Å resolution) with catalytic core in inactive down position. The UBE2C-binding site on APC11 RING domain is blocked with APC2-APC11 in down position previously described for apo-APC/C (Chang et al., 2014; Zhang et al., 2016).

(F) The left three panels show side-by-side pairwise comparison of density corresponding to APC2-APC11 catalytic core after superimposing cryo-EM maps for apo APC/C and APC/C^{CDC20} (Zhang et al., 2016) and APC/C^{CDC20}Δ15-MCC in the atypical inactive open configuration shown in (E). CDC20$_A$ binding to apo APC/C typically induces repositioning of the APC2-APC11 catalytic core from a down position to an up orientation, which enables UBE2C to bind APC2's WHB and APC11's RING domains (Brown et al., 2015; Chang et al., 2015; Zhang et al., 2016). The minor population of APC/C^{CDC20}Δ15-MCC in the open configuration is inactive due to the catalytic core occupying the down orientation. Right: APC2 WHB domain rotation between engaging MCC in closed conformation (green) or UBE2C for UB ligation (red).

(G) The ratio of CDC20$_A$-MCC populations in closed versus open configurations observed in negative-stain EM reconstructions of seven matched purifications of MCC bound to WT or Δ15 APC/C^{CDC20} (Table S2). Samples with no open classes are denoted (≈).

(H) Among the classes in open configurations analyzed in (G), the poplulations with the APC2-APC11 catalytic core in activated up versus inactive down positions were compared for WT or Δ15 APC/C^{CDC20} (Table S3).

(I) Comparing effects of MCC on WT or APC/C^{CDC20}Δ15-stimulated activation of UBE2C∼UB, as monitored by hydrolysis of oxyester-linked UBE2C(catalytic Cys-to-Ser)∼UB into free UBE2C and UB, is shown.

(J) Comparing MCC inhibition of WT or APC/C^{CDC20}Δ15-stimulated activation of UBE2C∼UB, by quantification of UBE2C∼UB remaining after 3 hr from experiments as in (I), is shown. Error, SEM; n = 3.

See also Figure S5 and Tables S2 and S3.

in resolution, with a lower resolution for catalytic core presumably arising from dynamic properties required for ubiquitination, The map resembled that representing an APC/C^{CDH1}-UBE2C∼UB-substrate intermediate, with UBE2C bound to APC2-APC11 adjacent to substrate and with the donor UB not visible presumably due to conformational flexibility (Figures S5C and S5D) (Brown et al., 2014, 2015; Zhang et al., 2016). The most obvious effects of deleting APC15 were the lack of

APC15 and disappearance of density for and rearrangement of APC15-binding helices from APC5 (Figure S5E).

We analyzed conformations of APC/C^{CDC20}Δ15-MCC by cryo-EM to understand how ubiquitination is impaired. Maps corresponding to closed and open configurations were refined at overall resolutions of 4.8 and 9 Å, respectively (Figures 5D, 5E, and S2A). In comparison to the WT complex, the complex lacking APC15 showed an obvious increase in the population of the $CDC20_M$-MCC assembly in the closed configuration, accompanied by relative rotation in APC4/APC5 regions (Figure S5E). This would block binding to UBE2C due to BUBR1 hijacking the WHB domain from APC2 (Figures 5D and 5F). UBE2C activation also was blocked in the less populated class with MCC in the open orientation, because APC2-APC11 was in the down position typically observed in apo-APC/C, which occludes UBE2C binding to the RING (Figures 2A, 5E, and 5F).

We tested if deleting APC15 indeed would hinder APC/C^{CDC20}-MCC-dependent activation of UBE2C. First, we obtained structural data by collecting negative-stain EM datasets, calculating maps, and quantifying populations in different conformations for 14 samples from seven matched preps with or without APC15. In the preps lacking APC15, the proportion forming the closed configuration was relatively increased, while those classes with the open $CDC20_A$-MCC configuration predominantly displayed the catalytic core in the down orientation blocked for UBE2C binding (Figures 5G and 5H; Tables S2 and S3). Second, we directly tested effects of deleting APC15 and/or adding MCC on the activation of UBE2C∼UB, by monitoring hydrolysis of an oxyester-bonded UBE2C∼UB conjugate with UB linked to Ser replacing UBE2C's catalytic Cys. In agreement with the structural data, adding APC/C^{CDC20} stimulated hydrolysis of the oxyester-bonded UBE2C∼UB conjugate irrespective of the presence or absence of APC15, while deleting APC15 enhanced inhibition by MCC (Figures 5I and 5J).

Although activity was greatly reduced, low-level hydrolysis of UBE2C∼UB (Figures 5I and 5J) raised the possibility that APC15 is not absolutely required for APC/C^{CDC20}-MCC to adopt a conformation that activates UBE2C∼UB. This may be enhanced or more detectable at high protein concentrations, such as those used in the hydrolysis assay. To test if APC/C^{CDC20}Δ15-MCC can indeed attain an active conformation with UBE2C, we assembled the crosslinked MCC-UBE2C complex with APC/C^{CDC20}Δ15 for structural analysis by negative-stain EM (Figure 6A). The map was strikingly similar to that from the corresponding complex with WT APC/C^{CDC20} (Figure 4E). Overall, the data suggest that APC/C^{CDC20}Δ15-MCC can, in principle, activate UBE2C∼UB but that the active conformation is not preferred.

Since the EM maps of APC/C^{CDC20}Δ15-MCC in the closed configuration uniformly showed APC2-APC11 in the activated up location but with UBE2C access blocked by MCC, we hypothesized that mutations disrupting key interactions unique to the closed configuration should enable activation of UBE2C∼UB and ubiquitination of $CDC20_M$, even by APC/C^{CDC20}Δ15. One interaction unique to the closed configuration involved MCC hijacking the UBE2C-binding surface of APC2's WHB domain (Figures 6A–6C). Another involved peptide-like density terminating in the available tetratricopeptide repeat (TPR) groove from APC8 (protomer A of the APC8 homodimer) (Figure 6D). We attributed this density to $CDC20_M$'s Ile-Arg (IR) tail, due to striking similarity to IR tails from APC10, CDH1, and $CDC20_A$ bound to TPR grooves from the two APC3 protomers (Figure S5F) (Chang et al., 2015; Zhang et al., 2016). Also, $APC8_A$ is, in principle, competent to bind an Ile and Arg, as protomer B contacts such residues within a coactivator's C-box motif (Chang et al., 2015; Zhang et al., 2016) (Figure S5F), while $APC8_A$ is poised to bind $CDC20_M$'s IR tail with MCC positioned in the closed configuration. Indeed, structure-based mutations in the BUBR1 surface that binds the APC2 WHB domain, or in $CDC20_M$'s IR tail, substantially restored the ability of APC/C^{CDC20}Δ15 to hydrolyze UBE2C∼UB in the presence of MCC (Figures 6E–6H) and to catalyze $CDC20_M$ ubiquitination (Figures 6I and 6J).

UBE2S-Dependent UB-Chain Synthesis in the Presence of MCC

To understand how MCC binding would affect UB chain formation, we inspected the cryo-EM maps for potential to form the specialized APC/C architecture juxtaposing UBE2S's active site with an acceptor UB. A prior cryo-EM reconstruction, obtained by crosslinking UBE2S's catalytic Cys to a substrate-fused UB variant (UBv) with enhanced affinity for the acceptor UB-binding site, indicated that UB chain elongation by UBE2S involves a completely different catalytic architecture from that activating UBE2C (Brown et al., 2016). Instead, UBE2S's C-terminal peptide (CTP) binds an APC2/APC4 groove, while UBE2S's catalytic domain contacts a pair of APC2 C/R domain helices. The unique interactions direct UBE2S's active site toward an acceptor UB recruited to a distinct APC11 RING surface (Brown et al., 2014, 2016; Kelly et al., 2014). Notably, prior data showed that MCC did not inhibit UBE2S-dependent synthesis of unanchored diUB chains with endogenous APC/C^{CDC20} (Kelly et al., 2014).

Even in the closed configuration of APC/C^{CDC20}-MCC, the UBE2S and acceptor UB-binding sites appeared available (Figures 7A and S6A) (Kelly et al., 2014). To test if UBE2S activity is spared with MCC predominantly bound in the closed configuration, we examined UBE2S-dependent UB transfer to a fluorescein-labeled acceptor UB*, and we saw no defect from deleting APC15 (Figure 7B). To visualize this, we adapted our published approach and performed cryo-EM on APC/C^{CDC20}Δ15-MCC bound to a complex with UBE2S's catalytic Cys crosslinked to the UBv as a proxy for an acceptor UB (Brown et al., 2016) (Figure 7C). A map for the closed configuration was refined at 5.7-Å resolution, which allowed placement of APC/C^{CDC20}Δ15-MCC, while the local resolution for the catalytic core was ≈10 Å (Figures 7D, S6A, and S6B; Table S1). The position of UBE2S-UBv was approximated based on prior cryo-EM data where UBE2S was more avidly anchored with the Ubv fused to a substrate (Figures 7D and S6A) (Brown et al., 2016).

The structural data confirmed that MCC blocks substrate-binding sites on $CDC20_A$ while allowing UBE2S placement adjacent to the UB-binding site on APC11's RING domain (Figure 7D). This led to several predictions. First, UBE2S should extend polyUB chains initiated by UBE2C and APC/C^{CDC20}-MCC. We confirmed this for $CDC20_M$, as higher molecular weight conjugates were observed upon adding UBE2S, but there was no

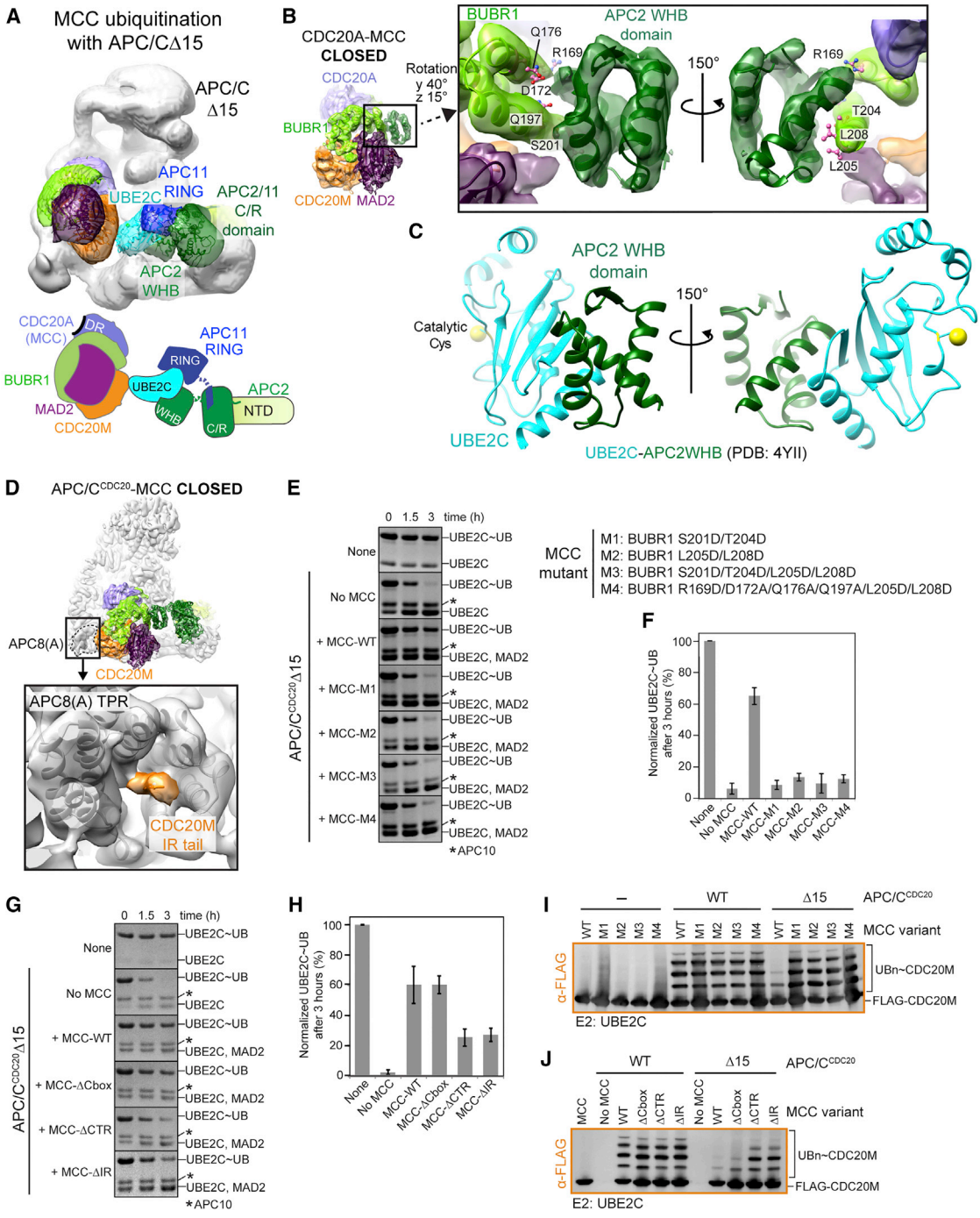

Figure 6. Elements Distinctly Mediating MCC Interactions with APC/C Subunits in Closed Configuration Determine Inhibition of $CDC20_M$ Ubiquitination

(A) APC15 is not absolutely required for APC/C^{CDC20}-UBE2C to adopt catalytic architecture for $CDC20_M$ ubiquitination. Negative-stain EM reconstruction of APC/C^{CDC20}Δ15-UBE2C-MCC core shows that forcing juxtaposition of UBE2C and $CDC20_M$ by crosslinking enables visualizing catalytic assembly as in Figure 4E.

(B) Close-up view shows BUBR1-APC2 WHB domain interactions distinctive for the closed configuration of APC/C^{CDC20}-MCC, with crystal structures (Bolanos-Garcia et al., 2011; Brown et al., 2015) docked in cryo-EM map from APC/C^{CDC20}Δ15-MCC and showing BUBR1 residues mutated in (E), (F), and (I).

(C) Crystal structure of APC2 WHB domain bound to UBE2C (Brown et al., 2015), oriented as APC2 WHB-domain-BUBR1 interface in (B), shows how MCC in closed configuration blocks UBE2C binding.

(D) Close-up view of APC8 (A) TPR pocket shows density attributed to $CDC20_M$ IR tail, an interaction unique to the closed configuration of APC/C^{CDC20}-MCC.

(E) Mutating APC2-binding residues from BUBR1 substantially restores APC/C^{CDC20}Δ15-stimulated hydrolysis of oxyester-linked UBE2C~UB.

(legend continued on next page)

modification by APC/C^{CDC20}Δ15 that inhibited UBE2C-dependent priming of $CDC20_M$ (Figures 7E and S6C). Second, if a substrate is already marked by a UB, such as a UB-Securin* fusion, then the level of UBE2S-dependent chain growth would reflect that occurring upon MCC inhibition of D- and KEN-box access to $CDC20_A$, irrespective of whether APC/C^{CDC20}-MCC was closed or open. Indeed, the products of APC/C^{CDC20}-UBE2S-catalyzed ubiquitination reactions were similar with UB-Securin* in the presence of MCC or a different competitor (Hsl1) blocking the D- and KEN-box sites on $CDC20_A$ or in the absence of MCC but with a D- and KEN-box mutant UB-Securin* (Figures S6D and S6E). Thus, MCC competes with substrate binding, but, if an acceptor UB is accessible, UBE2S can elongate chains even with $CDC20_A$-MCC in the closed configuration (Figure 7F).

DISCUSSION

Overall, our data define conformational control and reciprocal regulation of APC/C^{CDC20} and MCC (Figure 7G). First, the cryo EM data reveal elements blocking degron motifs from accessing APC/C^{CDC20}-MCC, explaining how substrate ubiquitination is inhibited (Figures 3 and S3). Second, a range of $CDC20_A$-MCC orientations, coupled with conformational dynamics of the APC/C catalytic core, endows APC/C^{CDC20}-MCC with variable functions. Although targeting with UBE2C is blocked when APC/C^{CDC20}-MCC is closed, the open configuration places $CDC20_M$ ubiquitination sites (Lys485 and Lys490) for modification by activated UBE2C (Figure 4E). Since MCC does not impair UBE2S association (Kelly et al., 2014), polyubiquitination could occur rapidly in cells after $CDC20_M$ is initially primed by UBE2C (Figure 7E).

At this point, how APC/C^{CDC20}-MCC conformations are naturally toggled remains poorly understood. The strong stabilization of APC/C-MCC upon checkpoint activation in cells depleted of APC15 (Foster and Morgan, 2012; Mansfeld et al., 2011; Uzunova et al., 2012) raises the possibility that activating the checkpoint may involve shifting APC/C^{CDC20}-MCC to closed or down configurations. By contrast, mechanisms opening APC/C^{CDC20}-MCC would increase UBE2C∼UB activation and ubiquitination of $CDC20_M$, much like our mutations removing contacts unique to the closed conformation (Figure 6). It seems that UBE2C access is a crucial determinant controlling the reciprocal regulation of APC/C^{CDC20} and MCC. Indeed, UBE2C is a mediator of checkpoint silencing (Jia et al., 2011; Reddy et al., 2007; Varetti et al., 2011). UBE2C could potentially act as a wedge capturing APC/C^{CDC20}-MCC as it swings open. APC/C^{CDC20}-MCC conformation also could be influenced by factors affecting the APC4-APC5 region, which resembles a lever arm poised as a conduit between $CDC20_A$-MCC and the catalytic core (Figure S5E). This could potentially be regulated by several phosphorylation sites in APC5, which are substituted by glutamates in our recombinant APC/C^{CDC20} (Qiao et al., 2016).

BUB3 also regulates termination of the checkpoint (Vanoosthuyse et al., 2009; Windecker et al., 2009), but it is not visible in the EM maps (Figure 1). Interestingly, BUB3-mediated checkpoint silencing may involve binding to M-E-L-phosphoT sequences, and we note that such a sequence invisible in APC5 in the cryo-EM maps is potentially positioned to modulate APC/C^{CDC20}-MCC conformation (Vleugel et al., 2015; Yamagishi et al., 2012). The overall similarity of EM maps for APC/C^{CDC20}-MCC complexes with or without BUB3 also raises the question as to whether UBE2C could ubiquitinate CDC20 in the context of assembly/disassembly intermediates containing only subsets of MCC components (Eytan et al., 2013; Han et al., 2013).

It seems likely that the configurations of APC/C^{CDC20}-MCC mediating various roles (inhibition, $CDC20_M$ ubiquitination, or other functions such as MCC dissociation) rely on multisite interactions, where each element is weak on its own but synergistic formation or dismantling of multiple contacts governs conformational control of distinctive activities. Multisite regulation is emerging as a common mechanism controlling APC/C activities, including EMI1 inhibition of interphase APC/C^{CDH1} (Chang et al., 2015; Frye et al., 2013; Miller et al., 2006; Wang and Kirschner, 2013), and recruitment, positioning, and activation of APC/C's partner E2s to achieve different forms of ubiquitination (Brown et al., 2014, 2015, 2016; Chang et al., 2015; Kelly et al., 2014). Multisite interactions also can allow E3 regulators to straddle multiple functions (Figure S7). MCC represents a distinct manifestation of E3 modulator, as pan-inhibitor or selective substrate of APC/C^{CDC20} as needed (Figure 7G). It seems likely that there will be many other cases where subtle variations in regulation can determine when a single E3 regulator is an inhibitor, substrate, or modulator of UB ligation to establish dynamic cellular regulation.

EXPERIMENTAL PROCEDURES

Proteins and Assays

Proteins used in this study were human except for yeast Hsl1. Recombinant APC/C and its variants contain 100 phosphomimetic mutations (Qiao et al., 2016; Weissmann et al., 2016). CDC20, MCC, and variants were expressed in Hi5 insect cells, and then they were purified by nickel affinity, cation exchange, and size exclusion chromatography.

Substrate ubiquitination assays were performed as described, with MCC titrated from 15 to 250 nM (Brown et al., 2016; Qiao et al., 2016). CDC20 ubiquitination assays were adapted from Foe et al. (2011) and Foster and Morgan (2012) to use methyl UB, and they were extended to include UBE2S with WT UB. To distinguish CDC20 ubiquitination targets, $CDC20_A$ and $CDC20_M$ were N-terminally Myc- and FLAG-tagged, respectively, for two-color western

(F) Comparing APC/C^{CDC20}Δ15-stimulated activation of UBE2C∼UB in the presence of WT or BUBR1 mutant MCC, by quantification of UBE2C∼UB remaining after 3 hr from experiments as in (E), is shown. Error, SEM; n = 3.

(G) Mutating IR tail from $CDC20_M$ in MCC, but not a negative control region (C-box), substantially restores APC/C^{CDC20}Δ15-stimulated hydrolysis of oxyester-linked UBE2C∼UB.

(H) Quantification of UBE2C∼UB after 3 hr from experiments as in (G) is shown. Error. SEM; n = 3.

(I) Mutating APC2-binding residues from BUBR1 restores $CDC20_M$ ubiquitination by APC/C^{CDC20}Δ15 and UBE2C.

(J) Mutating $CDC20_M$ IR tail restores ubiquitination by APC/C^{CDC20}Δ15 and UBE2C.

See also Figure S5.

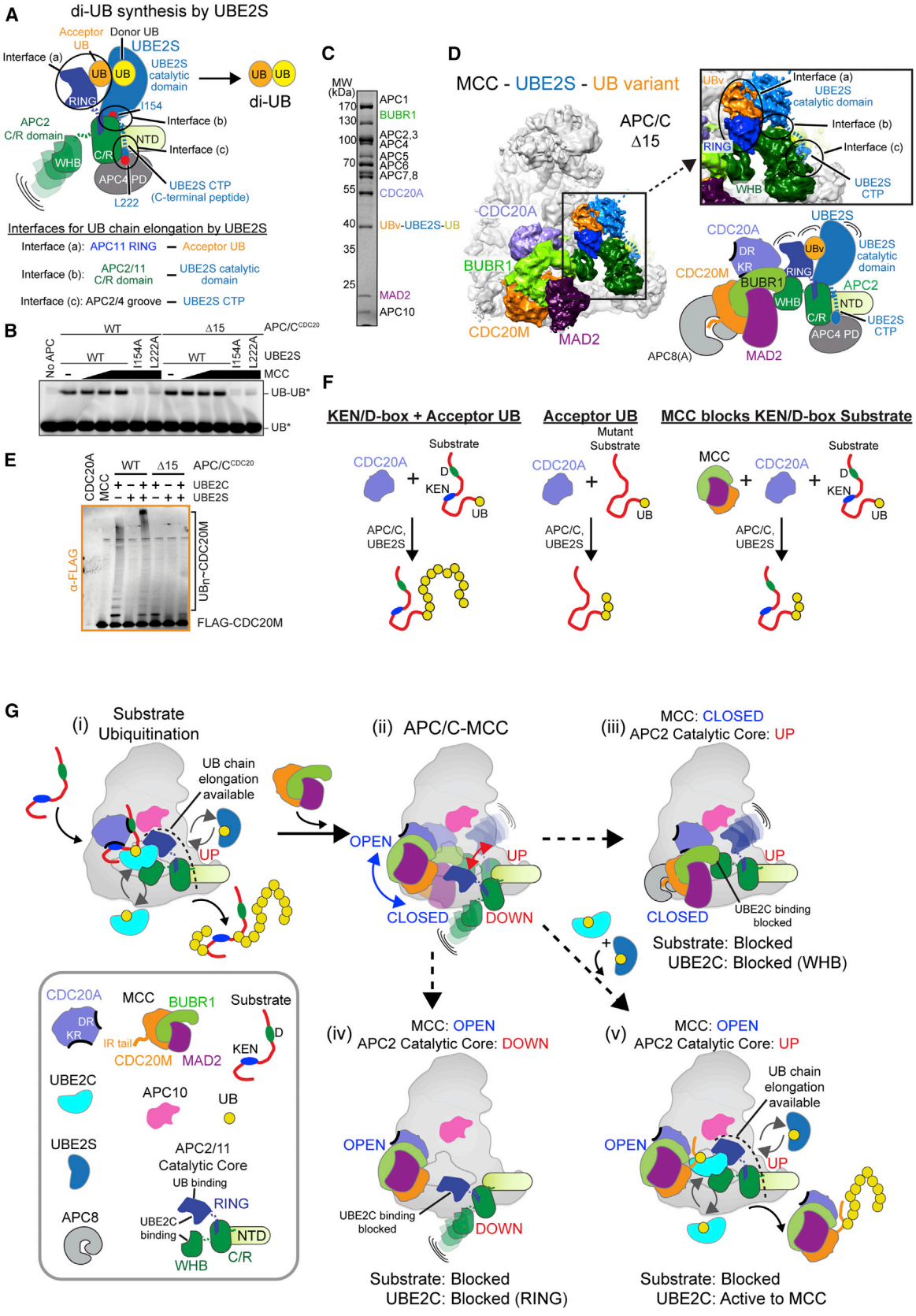

(legend on next page)

detection by secondary antibodies conjugated with DyLight 488 and Alexa 633, respectively, during a single scan with Typhoon FLA 9500.

Hydrolysis of oxyester-linked UBE2C∼UB (Brown et al., 2015) was performed three independent times, with 1 μM APC/C or APC/CΔ15, 1 μM CDC20, 5 μM UBE2C∼UB, and ±1 μM MCC at 30°C. Reaction products were visualized in Coomassie blue-stained 4%–12% NuPAGE gels (Life Technologies).

Complex Preparation for EM

Complexes were purified by sequential affinity pull-downs, followed by specific polishing steps. APC/C^{CDC20} and APC/C^{CDC20}-MCC, or versions lacking APC15, were prepared by either coexpressing APC/C, CDC20, and/or MCC or by mixing lysates from Hi5 insect cell cultures expressing components independently. Subcomplexes crosslinked to E2 active sites (UBE2C-substrate-UB [FLAG-tagged donor UB mimic], UBE2C-MCC [His_6-FLAG-tagged BUBR1], and UBE2S-UBv-UB [untagged]) were generated largely as described previously (Brown et al., 2015, 2016). Two- or three-way crosslinking between cysteine side chains was performed through the use of BMOE or TMEA (Pierce), respectively. Complexes were initially purified based on affinity tag(s) on APC/C, either a C-terminal Twin-Strep tag on APC4 or sequentially via an N-terminal Twin-Strep tag on APC2 and N-terminal GST tag on APC16. Complexes were enriched by FLAG affinity for BUBR1 or a donor UB mimic in some crosslinked complexes, with detailed purification procedures described in the Supplemental Experimental Procedures.

ACCESSION NUMBERS

The accession numbers for the data reported in this paper are Electron Microscopy Data Bank: EMD-4021, EMD-4022, EMD-4023, EMD-4024, EMD-4025, EMD-4026, EMD-4027, and EMD-4028 and Protein Data Bank: 5KHR and 5KHU.

SUPPLEMENTAL INFORMATION

Supplemental Information includes Supplemental Experimental Procedures, seven figures, three tables, and three movies and can be found with this article online at http://dx.doi.org/10.1016/j.molcel.2016.07.003.

AUTHOR CONTRIBUTIONS

M.Y., R.V., F.W., S.S.S., J.-M.P., H.S., and B.A.S. planned and supervised the project. M.Y., R.V., F.W., and R.Q. designed recombinant APC/C and MCC used herein. M.Y., R.V., N.G.B., and W.Z. performed biochemical analyses. M.Y., R.V., and N.G.B. made EM samples. P.D. and H.S. collected EM data, analyzed by M.Y., R.V., B.A.S., and H.S. with help from D.H. M.Y., R.V., J.-M.P., H.S., and B.A.S. prepared the paper.

ACKNOWLEDGMENTS

We thank M. Brunner, K.P. Wu, J.R. Michael, D.W. Miller, and S. Frase for advice and assistance. Funding was received from the Jane Coffin Childs Foundation, Leukemia & Lymphoma Society (N.G.B.); Austrian Science Fund FWF–Hertha Firnberg Program (R.Q.); Japan Society for the Promotion of Science (M.Y.); Canadian Institutes of Health Research (CIHR) MOP 111149 and 136956 (S.S.S.); Boehringer Ingelheim, the Austrian Science Fund (SFB-F34 and Wittgenstein award), the Austrian Research Promotion Agency (Headquarter grants FFG-832936 and FFG-852936 and Laura Bassi Centre for Optimized Structural Studies grant FFG-840283), and the European Community (FP7/2007-2013, grant 241548, MitoSys) (J.M.-P.); DFG Sonderforschungsbereich 860 (H.S.); and American Lebanese Syrian Associated Charities (ALSAC), NIH R37GM065930 and P30CA021765, and Howard Hughes Medical Institute (HHMI; B.A.S.).

Received: March 24, 2016
Revised: June 17, 2016
Accepted: July 7, 2016
Published: August 10, 2016

REFERENCES

Bolanos-Garcia, V.M., Lischetti, T., Matak-Vinković, D., Cota, E., Simpson, P.J., Chirgadze, D.Y., Spring, D.R., Robinson, C.V., Nilsson, J., and Blundell, T.L. (2011). Structure of a Blinkin-BUBR1 complex reveals an interaction crucial for kinetochore-mitotic checkpoint regulation via an unanticipated binding Site. Structure *19*, 1691–1700.

Braunstein, I., Miniowitz, S., Moshe, Y., and Hershko, A. (2007). Inhibitory factors associated with anaphase-promoting complex/cylosome in mitotic checkpoint. Proc. Natl. Acad. Sci. USA *104*, 4870–4875.

Brown, N.G., Watson, E.R., Weissmann, F., Jarvis, M.A., VanderLinden, R., Grace, C.R., Frye, J.J., Qiao, R., Dube, P., Petzold, G., et al. (2014). Mechanism of polyubiquitination by human anaphase-promoting complex: RING repurposing for ubiquitin chain assembly. Mol. Cell *56*, 246–260.

Brown, N.G., VanderLinden, R., Watson, E.R., Qiao, R., Grace, C.R., Yamaguchi, M., Weissmann, F., Frye, J.J., Dube, P., Ei Cho, S., et al. (2015). RING E3 mechanism for ubiquitin ligation to a disordered substrate visualized for human anaphase-promoting complex. Proc. Natl. Acad. Sci. USA *112*, 5272–5279.

Brown, N.G., VanderLinden, R., Watson, E.R., Weissmann, F., Ordureau, A., Wu, K.P., Zhang, W., Yu, S., Mercredi, P.Y., Harrison, J.S., et al. (2016). Dual RING E3 Architectures Regulate Multiubiquitination and Ubiquitin Chain Elongation by APC/C. Cell *165*, 1440–1453.

Figure 7. Multiple Catalytic and Conformational Mechanisms Contributing to Reciprocal Regulation of APC/C^{CDC20} and MCC

(A) Left: distinctive catalytic architecture for UBE2S-mediated diUB synthesis (Brown et al., 2016). Distinct surface of APC11 RING recruits acceptor UB. APC2 C/R domain activates UBE2S catalytic domain. APC2/APC4 (propeller domain [PD]) groove recruits UBE2S's unique C-terminal peptide (CTP). Key elements (APC11 RING UB-binding site, APC2-APC11 C/R domain, and APC2/APC4 groove) required for UB chain synthesis by UBE2S are available in the presence of MCC.

(B) Reactions with or without MCC monitoring WT or Δ15 APC/C^{CDC20} and UBE2S-catalyzed substrate-independent diUB* synthesis. UBE2S control mutants (I154A and L222A) confirm the role of catalytic architecture (Brown et al., 2014, 2016; Kelly et al., 2014).

(C) SDS-PAGE gel of purified APC/C^{CDC20}Δ15 complex with MCC core and three-way UBE2S-UBv-UB complex to represent UB chain elongation. UBv is a UB variant with enhanced affinity for the acceptor UB-binding surface of APC11 RING (Brown et al., 2016).

(D) Cryo-EM map shows complex from (C), representing overall conformational compatibility for UBE2S-dependent UB chain formation with APC/C^{CDC20}Δ15-MCC in the closed configuration.

(E) Experiment tests if UBE2S catalyzes UB chain elongation on MCC's $CDC20_M$ in the presence of UBE2C and either WT APC/C^{CDC20} or the mutant lacking APC15.

(F) Summary of (B)–(E) and Figures S6C and S6D. MCC inhibits D/KEN recruitment, but not intrinsic chain-forming activity of APC/C^{CDC20}-UBE2S, irrespective of APC15-dependent conformational modulation.

(G) Conformations of APC/C^{CDC20}-MCC determine reciprocal regulation. MCC degron-like elements mediate binding to $CDC20_A$ to inhibit substrate ubiquitination (i and ii). Rotation of the $CDC20_A$-MCC assembly and APC/C conformation determine if UBE2C is blocked from the APC2-APC11 catalytic core (iii and iv) or if CDC20 can be ubiquitinated by UBE2C (v). After an initial UB is linked, a UB chain can be extended by UBE2S.

See also Figures S6 and S7.

Burton, J.L., and Solomon, M.J. (2007). Mad3p, a pseudosubstrate inhibitor of APCCdc20 in the spindle assembly checkpoint. Genes Dev. *21*, 655–667.

Burton, J.L., Tsakraklides, V., and Solomon, M.J. (2005). Assembly of an APC-Cdh1-substrate complex is stimulated by engagement of a destruction box. Mol. Cell *18*, 533–542.

Chang, L., Zhang, Z., Yang, J., McLaughlin, S.H., and Barford, D. (2014). Molecular architecture and mechanism of the anaphase-promoting complex. Nature *513*, 388–393.

Chang, L., Zhang, Z., Yang, J., McLaughlin, S.H., and Barford, D. (2015). Atomic structure of the APC/C and its mechanism of protein ubiquitination. Nature *522*, 450–454.

Chao, W.C., Kulkarni, K., Zhang, Z., Kong, E.H., and Barford, D. (2012). Structure of the mitotic checkpoint complex. Nature *484*, 208–213.

Di Fiore, B., Davey, N.E., Hagting, A., Izawa, D., Mansfeld, J., Gibson, T.J., and Pines, J. (2015). The ABBA motif binds APC/C activators and is shared by APC/C substrates and regulators. Dev. Cell *32*, 358–372.

Diaz-Martinez, L.A., Tian, W., Li, B., Warrington, R., Jia, L., Brautigam, C.A., Luo, X., and Yu, H. (2015). The Cdc20-binding Phe box of the spindle checkpoint protein BubR1 maintains the mitotic checkpoint complex during mitosis. J. Biol. Chem. *290*, 2431–2443.

Eytan, E., Sitry-Shevah, D., Teichner, A., and Hershko, A. (2013). Roles of different pools of the mitotic checkpoint complex and the mechanisms of their disassembly. Proc. Natl. Acad. Sci. USA *110*, 10568–10573.

Foe, I.T., Foster, S.A., Cheung, S.K., DeLuca, S.Z., Morgan, D.O., and Toczyski, D.P. (2011). Ubiquitination of Cdc20 by the APC occurs through an intramolecular mechanism. Curr. Biol. *21*, 1870–1877.

Foley, E.A., and Kapoor, T.M. (2013). Microtubule attachment and spindle assembly checkpoint signalling at the kinetochore. Nat. Rev. Mol. Cell Biol. *14*, 25–37.

Foster, S.A., and Morgan, D.O. (2012). The APC/C subunit Mnd2/Apc15 promotes Cdc20 autoubiquitination and spindle assembly checkpoint inactivation. Mol. Cell *47*, 921–932.

Fraschini, R., Beretta, A., Sironi, L., Musacchio, A., Lucchini, G., and Piatti, S. (2001). Bub3 interaction with Mad2, Mad3 and Cdc20 is mediated by WD40 repeats and does not require intact kinetochores. EMBO J. *20*, 6648–6659.

Frye, J.J., Brown, N.G., Petzold, G., Watson, E.R., Grace, C.R., Nourse, A., Jarvis, M.A., Kriwacki, R.W., Peters, J.M., Stark, H., and Schulman, B.A. (2013). Electron microscopy structure of human APC/C(CDH1)-EMI1 reveals multimodal mechanism of E3 ligase shutdown. Nat. Struct. Mol. Biol. *20*, 827–835.

Fujimitsu, K., Grimaldi, M., and Yamano, H. (2016). Cyclin-dependent kinase 1-dependent activation of APC/C ubiquitin ligase. Science *352*, 1121–1124.

Garnett, M.J., Mansfeld, J., Godwin, C., Matsusaka, T., Wu, J., Russell, P., Pines, J., and Venkitaraman, A.R. (2009). UBE2S elongates ubiquitin chains on APC/C substrates to promote mitotic exit. Nat. Cell Biol. *11*, 1363–1369.

Ge, S., Skaar, J.R., and Pagano, M. (2009). APC/C- and Mad2-mediated degradation of Cdc20 during spindle checkpoint activation. Cell Cycle *8*, 167–171.

Han, J.S., Holland, A.J., Fachinetti, D., Kulukian, A., Cetin, B., and Cleveland, D.W. (2013). Catalytic assembly of the mitotic checkpoint inhibitor BubR1-Cdc20 by a Mad2-induced functional switch in Cdc20. Mol. Cell *51*, 92–104.

Hardwick, K.G., Johnston, R.C., Smith, D.L., and Murray, A.W. (2000). MAD3 encodes a novel component of the spindle checkpoint which interacts with Bub3p, Cdc20p, and Mad2p. J. Cell Biol. *148*, 871–882.

He, J., Chao, W.C., Zhang, Z., Yang, J., Cronin, N., and Barford, D. (2013). Insights into degron recognition by APC/C coactivators from the structure of an Acm1-Cdh1 complex. Mol. Cell *50*, 649–660.

Herzog, F., Primorac, I., Dube, P., Lenart, P., Sander, B., Mechtler, K., Stark, H., and Peters, J.M. (2009). Structure of the anaphase-promoting complex/cyclosome interacting with a mitotic checkpoint complex. Science *323*, 1477–1481.

Izawa, D., and Pines, J. (2015). The mitotic checkpoint complex binds a second CDC20 to inhibit active APC/C. Nature *517*, 631–634.

Jia, L., Li, B., Warrington, R.T., Hao, X., Wang, S., and Yu, H. (2011). Defining pathways of spindle checkpoint silencing: functional redundancy between Cdc20 ubiquitination and p31(comet). Mol. Biol. Cell *22*, 4227–4235.

Jia, L., Kim, S., and Yu, H. (2013). Tracking spindle checkpoint signals from kinetochores to APC/C. Trends Biochem. Sci. *38*, 302–311.

Kelly, A., Wickliffe, K.E., Song, L., Fedrigo, I., and Rape, M. (2014). Ubiquitin chain elongation requires E3-dependent tracking of the emerging conjugate. Mol. Cell *56*, 232–245.

Kim, S., and Yu, H. (2011). Mutual regulation between the spindle checkpoint and APC/C. Semin. Cell Dev. Biol. *22*, 551–558.

Kimata, Y., Baxter, J.E., Fry, A.M., and Yamano, H. (2008). A role for the Fizzy/Cdc20 family of proteins in activation of the APC/C distinct from substrate recruitment. Mol. Cell *32*, 576–583.

Kulukian, A., Han, J.S., and Cleveland, D.W. (2009). Unattached kinetochores catalyze production of an anaphase inhibitor that requires a Mad2 template to prime Cdc20 for BubR1 binding. Dev. Cell *16*, 105–117.

Lara-Gonzalez, P., Westhorpe, F.G., and Taylor, S.S. (2012). The spindle assembly checkpoint. Curr. Biol. *22*, R966–R980.

London, N., and Biggins, S. (2014). Signalling dynamics in the spindle checkpoint response. Nat. Rev. Mol. Cell Biol. *15*, 736–747.

Mansfeld, J., Collin, P., Collins, M.O., Choudhary, J.S., and Pines, J. (2011). APC15 drives the turnover of MCC-CDC20 to make the spindle assembly checkpoint responsive to kinetochore attachment. Nat. Cell Biol. *13*, 1234–1243.

Miller, J.J., Summers, M.K., Hansen, D.V., Nachury, M.V., Lehman, N.L., Loktev, A., and Jackson, P.K. (2006). Emi1 stably binds and inhibits the anaphase-promoting complex/cyclosome as a pseudosubstrate inhibitor. Genes Dev. *20*, 2410–2420.

Miniowitz-Shemtov, S., Teichner, A., Sitry-Shevah, D., and Hershko, A. (2010). ATP is required for the release of the anaphase-promoting complex/cyclosome from inhibition by the mitotic checkpoint. Proc. Natl. Acad. Sci. USA *107*, 5351–5356.

Musacchio, A. (2015). The molecular biology of spindle assembly checkpoint signaling dynamics. Curr. Biol. *25*, R1002–R1018.

Musacchio, A., and Ciliberto, A. (2012). The spindle-assembly checkpoint and the beauty of self-destruction. Nat. Struct. Mol. Biol. *19*, 1059–1061.

Nilsson, J., Yekezare, M., Minshull, J., and Pines, J. (2008). The APC/C maintains the spindle assembly checkpoint by targeting Cdc20 for destruction. Nat. Cell Biol. *10*, 1411–1420.

Pan, J., and Chen, R.H. (2004). Spindle checkpoint regulates Cdc20p stability in Saccharomyces cerevisiae. Genes Dev. *18*, 1439–1451.

Primorac, I., and Musacchio, A. (2013). Panta rhei: the APC/C at steady state. J. Cell Biol. *201*, 177–189.

Qiao, R., Weissmann, F., Yamaguchi, M., Brown, N.G., VanderLinden, R., Imre, R., Jarvis, M.A., Brunner, M.R., Davidson, I.F., Litos, G., et al. (2016). Mechanism of APC/CCDC20 activation by mitotic phosphorylation. Proc. Natl. Acad. Sci. USA *113*, E2570–E2578.

Reddy, S.K., Rape, M., Margansky, W.A., and Kirschner, M.W. (2007). Ubiquitination by the anaphase-promoting complex drives spindle checkpoint inactivation. Nature *446*, 921–925.

Sivakumar, S., and Gorbsky, G.J. (2015). Spatiotemporal regulation of the anaphase-promoting complex in mitosis. Nat. Rev. Mol. Cell Biol. *16*, 82–94.

Sudakin, V., Chan, G.K., and Yen, T.J. (2001). Checkpoint inhibition of the APC/C in HeLa cells is mediated by a complex of BUBR1, BUB3, CDC20, and MAD2. J. Cell Biol. *154*, 925–936.

Tian, W., Li, B., Warrington, R., Tomchick, D.R., Yu, H., and Luo, X. (2012). Structural analysis of human Cdc20 supports multisite degron recognition by APC/C. Proc. Natl. Acad. Sci. USA *109*, 18419–18424.

Uzunova, K., Dye, B.T., Schutz, H., Ladurner, R., Petzold, G., Toyoda, Y., Jarvis, M.A., Brown, N.G., Poser, I., Novatchkova, M., et al. (2012). APC15

mediates CDC20 autoubiquitylation by APC/C(MCC) and disassembly of the mitotic checkpoint complex. Nat. Struct. Mol. Biol. *19*, 1116–1123.

Van Voorhis, V.A., and Morgan, D.O. (2014). Activation of the APC/C ubiquitin ligase by enhanced E2 efficiency. Curr. Biol. *24*, 1556–1562.

Vanoosthuyse, V., Meadows, J.C., van der Sar, S.J., Millar, J.B., and Hardwick, K.G. (2009). Bub3p facilitates spindle checkpoint silencing in fission yeast. Mol. Biol. Cell *20*, 5096–5105.

Varetti, G., Guida, C., Santaguida, S., Chiroli, E., and Musacchio, A. (2011). Homeostatic control of mitotic arrest. Mol. Cell *44*, 710–720.

Vleugel, M., Omerzu, M., Groenewold, V., Hadders, M.A., Lens, S.M., and Kops, G.J. (2015). Sequential multisite phospho-regulation of KNL1-BUB3 interfaces at mitotic kinetochores. Mol. Cell *57*, 824–835.

Wang, W., and Kirschner, M.W. (2013). Emi1 preferentially inhibits ubiquitin chain elongation by the anaphase-promoting complex. Nat. Cell Biol. *15*, 797–806.

Weissmann, F., Petzold, G., VanderLinden, R., Huis In 't Veld, P.J., Brown, N.G., Lampert, F., Westermann, S., Stark, H., Schulman, B.A., and Peters, J.M. (2016). biGBac enables rapid gene assembly for the expression of large multisubunit protein complexes. Proc. Natl. Acad. Sci. USA *113*, E2564–E2569.

Wild, T., Larsen, M.S., Narita, T., Schou, J., Nilsson, J., and Choudhary, C. (2016). The spindle assembly checkpoint is not essential for viability of human cells with genetically lowered APC/C activity. Cell Rep. *14*, 1829–1840.

Williamson, A., Wickliffe, K.E., Mellone, B.G., Song, L., Karpen, G.H., and Rape, M. (2009). Identification of a physiological E2 module for the human anaphase-promoting complex. Proc. Natl. Acad. Sci. USA *106*, 18213–18218.

Windecker, H., Langegger, M., Heinrich, S., and Hauf, S. (2009). Bub1 and Bub3 promote the conversion from monopolar to bipolar chromosome attachment independently of shugoshin. EMBO Rep. *10*, 1022–1028.

Yamagishi, Y., Yang, C.H., Tanno, Y., and Watanabe, Y. (2012). MPS1/Mph1 phosphorylates the kinetochore protein KNL1/Spc7 to recruit SAC components. Nat. Cell Biol. *14*, 746–752.

Zhang, S., Chang, L., Alfieri, C., Zhang, Z., Yang, J., Maslen, S., Skehel, M., and Barford, D. (2016). Molecular mechanism of APC/C activation by mitotic phosphorylation. Nature *533*, 260–264.